Green Chemistry

PAPER

View Article Online
View Journal | View Issue



Cite this: *Green Chem.*, 2024, **26**, 11222

# Production of nanochitins *via* a shell biorefinery process for self-assembly applications as photonic films and Pickering emulsions†

Xuhai Zhu, ‡[a] Fuyan Peng,‡[a,b] Hui Li,[c] Rongjun Lin,[a,b] Rui Lu [a] and Fang Lu *[a]

The concept of sustainable development is driving shell biorefineries to develop a cost-effective and environmentally benign approach to transform chitin into high-value products. This study describes a green, simple, and flexible shell biorefinery process for producing two kinds of nanochitins (NCh), chitin solid residues (ChSRs) and chitin nanocrystals (ChNCs), by using *p*-toluenesulfonic acid-assisted hydrothermal treatment. The ChSR is a bundled nanocrystal with a long length ranging from 100 nm to 450 nm and a width ranging from 10 nm to 30 nm. It has an excellent interfacial behavior between the water and oil phases due to its amphiphilic nature; thus, a foodstuff-related emulsion has been successfully fabricated from soybean oil and a ChSR suspension without the addition of any synthetic surfactants. The further hydrolysed ChNC with a length and width range of 25–225 nm and 15–30 nm, respectively, and a high zeta potential of 41 mV exists as an individual nanocrystal. Owing to the abundance of positively charged groups distributed on its surface, ChNC enables self-assembly to a highly ordered hierarchical structure. Hence, ChNCs show promising results in fabricating large-area photonic films, *e.g.* for application in bright and vivid automobile painting. Altogether, we provide a novel approach to produce NCh materials from crustacean shell waste and bridge the gap from process engineering to high-value product development.

Received 3rd June 2024,
Accepted 30th September 2024

DOI: 10.1039/d4gc02680b

rsc.li/greenchem



## 1 Introduction

Crustacean shell waste is one of a few potential sources of biomass energy, but not the only one; there are other alternatives, such as wood, agricultural straw, poultry and livestock excrement, kitchen waste, *etc.*[1] Large amounts of crustacean waste are generated annually, especially the shells from seafood (*e.g.*, shrimps, crabs, and lobsters).[2] Therefore, utilizing shell biomass components for high-value chemicals/materials can be economically profitable and essential in addressing UN sustainability goals.[3] The main goal of the shell biorefinery approach is to maximize technical and, therefore, economic outcomes, considering high-value products from all biomass components. The shells are composed of three dominant components, *i.e.* 20–40% of protein, 20–50% of $CaCO_3$, and 15–40% of chitin.[4] Proteins have nutrient value and can be processed as fertilizers or animal feed, while biological organism-originated $CaCO_3$ is suitable for application in the biomedical field.[5] Chitin, poly(β-(1 → 4)-*N*-acetyl-D-glucosamine), is the second most abundant biopolymer after cellulose, primarily used in its highly degraded and deacetylated form, known as chitosan.[6] However, chitosan production with abundant waste and low profits can be seen as a limitation to the sustainable use of chitin, which justifies the consideration of new strategies with better environmental and economic prospects.[7,8]

Taking advantage of the novel characteristics of biomaterials at the nanoscale, simple top-down strategies have been applied to isolate their building blocks. In this context, studies on the preparation, characterization, and applications of chitin nanoparticles, referred to as "nanochitin (NCh)", have been extensively conducted.[8–10] Similar to producing nanocellulose from native celluloses, methods such as acid hydrolysis, pretreatments combined with mechanical disintegration, and chemical oxidations are generally employed to produce NCh from purified chitin.[10–13] The main challenges that hinder the industrialization of these technologies are three aspects. The first obstacle is the highly tunable processing conditions of the commonly

[a]*State Key Laboratory of Catalysis, Dalian Institute of Chemical Physics, Chinese Academy of Sciences, Dalian, Liaoning 110623, China. E-mail: lufang@dicp.ac.cn; Tel: +86-0411-8437-9846*
[b]*Henan Institute of Advanced Technology, Zhengzhou University, Zhengzhou, Henan 450052, China*
[c]*Zhengzhou Tobacco Research Institute, China National Tobacco Corporation, Zhengzhou, Henan 450001, China*

†Electronic supplementary information (ESI) available. See DOI: https://doi.org/10.1039/d4gc02680b

‡These authors equally contributed to this work.

used acid hydrolysis on chitin, which requires significant time and resources to learn the connections between processing conditions and output versatility regarding the NCh structure, yield, and physicochemical properties. To make the manufacture of NCh efficient and more profitable, kinetics-related processing parameters, like reaction temperature, time, and acid concentration, must be optimized to ensure that the properties of the extracted NCh are ideal for the intended end product.[14] The second one is chemical recovery and NCh product treatment, which often involve a multistage recovery. Generally, strong acids (sulfuric acid, hydrochloric acid, or nitric acid) or oxidation reagents (TEMPO, NaClO, $H_2O_2$) are utilized to catalyse the liberation of NCh from chitin.[10–14] However, the non-recyclability of these catalysts increases the production cost and harms the environment. Even though the production of thermally stable and functional nanocellulose by concentrated organic acid hydrolysis has been reported,[15] crustacean waste is different in composition from lignocellulosic waste; thus, using easily recoverable and reusable organic acids is a desirable technique for shell biorefineries. The last one is the manufacture of NCh directly from crustacean shells, which involves several cumbersome steps, including the intensive use of strong mineral acids to decompose $CaCO_3$ and NaOH to peel off protein, followed by using $NaClO_2$ to bleach and purify resultant chitins, and finally, isolation of chitin's building blocks at the nanoscale.[11,16] This extra chitin fractionation and purification necessitates expenditure on corrosion-resistant equipment and wastewater treatment; therefore, for further commercial applications, it would be desirable to improve the cost-effectiveness of the process and prepare NCh directly from the crustacean biomass. An acidic ionic liquid was recently made for *in situ* production of individual chitin nanowhiskers with low yield straight from shrimp shells.[17] In addition, various types of solid organic acids such as *p*-toluenesulfonic acid (PTSA), oxalic acid, maleic acid, malonic acid, tartaric acid, and citric acid were introduced to the hydrolysis treatment on biopolymers.[15,18,19] Inspired by the pressure cooker used to tenderize meat protein, a new fractionation method was recently reported to extract high-value chitin from shrimp shells using acidic hydrothermal treatment.[16] Based on these backgrounds, we are interested in evaluating the feasibility of solid organic acids as acid catalysts for NCh prepared straight from crustacean biomass by hydrothermal treatment.

The present work describes a green, simple, and flexible shell biorefinery process for producing NCh by solid organic acid-assisted hydrothermal treatment. The effect of reaction conditions, including solid organic acid types, temperature, time, and the molar ratio of acid to chitin, on the hydrolysis efficiency of purified chitin is first studied to identify the optimal hydrolysis conditions. Then, we proceed with the hydrolysis of crustacean shell waste. It is envisaged that a high quantity of NCh can be produced from crustacean shells in one pot by using hot water for deproteinization, solid organic acids for demineralization, and deliberation of chitin microfibrils. Furthermore, the recyclability and reusability of solid organic acids are evaluated. The morphology, chemical structure, and properties of the obtained NCh products are also characterized. Finally, the applications associated with the assembly behavior of the resultant NCh products are investigated. The biobased nanoparticles can generate complex structures *via* self-assembly guided by forces acting at multiple scales, of which functions and applications are determined by the nature of the particles and the assembly process.[8,9,14] Depending on the processing conditions of chitin hydrolysis, it is possible to adjust the characteristics of the resultant NCh particles for final applications associated with assembled structures.[8,9,14] It is, therefore, desirable to consider the process–property–application relationships involved in NCh for material design and development.

Overall, the main objectives of this work are (1) to study the effect of process conditions on the yield, structure, and physicochemical properties of the NCh products to evaluate the ability to engineer precursors with desirable characteristics; (2) to produce NCh products directly from the raw shell biomass and elucidate their properties; (3) to evaluate the application potential for the assembly behavior of NCh products.

# 2 Methods

## 2.1 Preparation of NCh from purified chitin

**Exploration of organic acids.** Six solid organic acids (PTSA, oxalic acid, maleic acid, malonic acid, tartaric acid, and citric acid) were selected to prepare NCh, respectively. In detail, a commercial chitin powder (1.0 g) was added with 20.0 g of aqueous acid in a 50 mL Teflon-lined stainless autoclave reactor (T316 stainless steel). These experiments have an identical value of 1.2 for the molar ratio of acid to *N*-acetylglucosamine (GlcNAc) of chitin, termed *n*(acid)/*n*(GlcNAc) = 1.2. The autoclave was sealed, purged three times with $N_2$ to expel air, and filled with 0.5 atm $N_2$ at room temperature. Subsequently, the autoclave was heated at 130 °C for four hours under the stirring of 200 rpm. After the reaction, the autoclave was removed from the heating source and cooled to room temperature by cooling water. The product mixture was centrifuged at 22 000*g* for 5 min, and the supernatant was removed by decantation. The resultant water-insoluble fraction was re-suspended in water, followed by dialysis against deionized water until a fairly steady pH was reached. Once again, the suspension was centrifuged at 22 000*g* for 5 min to obtain two types of NCh products as separate streams: chitin nanocrystals (ChNCs) and chitin solid residues (ChSRs). ChNC formed a stable suspension in the supernatant, whereas ChSR was obtained as a residue. Volumes and weights of each fraction were recorded, and samples were stored at 4 °C until further use. ChNC and ChSR yields were determined using the gravimetric method of oven-drying, where samples were dried at 105 °C until constant weight (eqn (1)):

$$\text{Yield}(\%) = \frac{m}{M} \times 100 \quad (1)$$

where $m$ is the dry weight of total ChNC or ChSR obtained (g), and $M$ is the dry weight of the starting material.

**Optimization of acid hydrolysis conditions.** The Box–Wilson central composite design (CCD) of response surface methodology was employed for experimental design to determine the optimum conditions of NCh production. Three factors, *i.e.*, the molar ratio of used acid and GlcNAc in chitin ($n$(acid)/$n$(GlcNAc)), hydrolysis duration (h), hydrolysis temperature (°C), and three responses, *i.e.*, ChNC, ChSR, and total yields, were evaluated. Based on exploratory single-factor experiments, the proper ranges of the three independent variables were $n$(acid)/$n$(GlcNAc) $X_1$ (0.6, 0.9, and 1.2), hydrolysis duration $X_2$ (2, 4, and 6 h) and hydrolysis temperature $X_3$ (100, 115, and 130 °C). The total number of experiments was 17, calculated using the formula: $N = 2k\,(k-1) + r$ (center points), where the number of factors ($k$) was 3 and the replicates of center point conditions ($r$) were 5. All experiments were conducted randomly to minimize the effect of unexpected variability in the observed response due to extraneous factors. Center point conditions were replicated to evaluate the experimental error. The optimal conditions were obtained once the maximized value of the production yield was found.

An actual experiment followed the optimized conditions to verify the predicted production yield. The experimental operations were the same as in the above paragraph. After the hydrolysis reaction, the water-soluble fraction collected from the product's suspension by centrifugation was stored for the subsequent acid recovery and reusing experiment. Some of the ChNC and ChSR products were freeze-dried for analyses, respectively, and the rest were stored at 4 °C before further use.

**Acid recycling and reuse.** The resultant supernatant containing PTSA from the above experiment was concentrated in a vacuum, and 30 mL of ethyl acetate (EtOAc) was added to dissolve PTSA at 50 °C. Due to its EtOAc insolubility, the produced sugar was separated *via* a simple filtration process. Then, the filtrate was concentrated using a rotary evaporator and dried. After that, high-purity PTSA was collected (R-PTSA). The recyclability of PTSA was assessed according to the recovery and purity of R-PTSA. The purity of R-PTSA was checked by the NMR technique. The recovery yield of R-PTSA was determined using eqn (2):

$$\text{Recovery yield}(\%) = \frac{m_r}{m_o} \times 100 \quad (2)$$

where $m_r$ and $m_o$ are the mass of R-PTSA and the original PTSA, respectively.

The reproducibility and reusability of R-PTSA were evaluated under the optimal conditions at which the maximum yields of ChNC and ChSR were collected. The corresponding ChNC and ChSR production yields were calculated. Some of the ChNC products were freeze-dried for analysis.

### 2.2 Preparation of NCh from crustacean biomass waste

Before hydrolysis, all shell samples were milled to pass through a 60-mesh screen in a Wiley mill to ensure particle size uniformity and increase surface area. Considering the variation in the composition and density of shell structure in these crustacean biomass wastes, they were subjected to hydrolysis following a procedure modified from the above optimal conditions. This process can realize the demineralization, deproteinization, and NCh production in one pot.

In a typical experiment for crab shells, 1.0 g of shell powder, 1.8 g of PTSA, 17.2 g of deionized water, and a stirrer bar were placed in a Teflon-lined autoclave with 50 mL inner volume. The mixture was capped and demineralized at room temperature with constant stirring for 12 h. During this procedure, a large amount of foam can be observed. Afterward, an additional 1.8 g of PTSA was added, and the autoclave was sealed and filled with 0.5 atm $N_2$. The reaction was stirred and subjected to 120 °C heating. To ensure that proteins can be extracted sufficiently by the acid-catalyzed hydrothermal treatment and that chitin fiber thus released can be hydrolysed into the NCh product, the reaction time was extended to 12 h. After the reaction, the product mixture was separated by using a centrifuge (22 000*g*, 5 min). The solid residue was washed thoroughly with water by repeated centrifugation, followed by dialysis against deionized water until a fairly steady pH was reached. Finally, ultrasound treatment was conducted to disperse the NCh particles derived from crab shells ($NCh_{crab}$). The NCh products from crawfish ($NCh_{crawfish}$) and shrimp ($NCh_{shrimp}$) shells followed the same general protocol as the $NCh_{crab}$, the only difference being the added amount of PTSA. In the production of $NCh_{crawfish}$, 0.9 g and 1.8 g of PTSA were added in the demineralization and acid-catalyzed hydrothermal steps, respectively. In contrast, a lower amount of PTSA (0.9 g) was used in the acid-catalyzed hydrothermal reaction to produce $NCh_{shrimp}$. The remaining steps of the preparation protocol are the same as those for the $NCh_{crab}$. The overall mass yield of NCh from biomass was calculated based on the chitin available in biomass, and some NCh products were freeze-dried for analysis.

### 2.3 Application of NCh products

**Fabrication of photonic films with ChNC.** ChNC-based photonic films were obtained using the spray-painting method. Initially, concentrated ChNC gel was diluted to 50 mL by adding Milli-Q water, generating a homogeneous suspension with a concentration of 1.0 wt%. Then, polyvinyl alcohol (PVA) was dissolved in diluted ChNC suspension with a mass ratio of 2 : 1 w/w to obtain ChNC/PVA suspensions after sonication. The mixture suspension was vigorously stirred overnight at room temperature and then transferred to a tank of paint spray gun. The ChNC/PVA composite films were obtained by spraying the resulting suspension on the 201-type stainless-steel plates with different sizes. Each film's characteristic color can be observed after drying for 30 min at room temperature.

**Production of Pickering emulsion gels with ChSR.** Suspensions of various ChSR concentrations (0.2, 0.4, 0.6, 0.8, 1.0, and 1.4 wt%) were prepared by dilution for further use. A series of 10 g water-continuous emulsion gels were prepared by mixing soybean oil with the above suspensions in different mass ratios of oil to water (8 : 2, 7 : 3, 6 : 4, 5 : 5, and 4 : 6) with a high-speed shear homogenizer (T-118 Ultra-Turrax, IKA, Germany) at a shear rate of 20 000 rpm for 3 min. Optical photographs of

 

emulsions were taken after storage at room temperature for 7 days. During this period, the emulsion separation was quantified based on the Emulsion Index (EI, eqn (3)):

$$\mathrm{EI}(\%) = \left(\frac{H_c}{H_t}\right) \times 100 \quad (3)$$

where $H_c$ is the height of emulsion phase, and $H_t$ is the total height of the suspension system.

To simultaneously visualize ChSR and soybean oil, emulsification was done using soybean oil dyed with Nile red and ChSR stained with fluorescein isothiocyanate (FITC). Nile red solution (1 mg $mL^{-1}$ in isopropyl alcohol) was mixed with soybean oil at a mass ratio of 1/25, which was thoroughly stirred overnight at room temperature; FITC solution (1 mg $mL^{-1}$ in isopropyl alcohol) was stirred with ChSR at a mass ratio of 1/25 overnight at room temperature. The oil-to-water ratio was set as 7/3, and the 1.0 wt% of stained ChSR was used, wherein the mixture was emulsified following the above procedures. The labelled emulsions were stored at 4 °C before characterization.

# 3 Results and discussion

## 3.1 General

Fig. 1 illustrates the entire experimental process flow for producing NCh products with minimum chitin loss by organic acid-assisted hydrothermal treatment followed by centrifuge fractionation. In this work, crystalline solid-type organic acids were applied to hydrolyse the purified chitin to gently destroy the chemical bonds of the feed chitin under mild conditions and enhance the yield of NCh under mild acid hydrolysis conditions. The hydrolysis reaction was carried out using acids over a range of molar ratio of acid to *N*-acetylglucosamine of chitin ($n$(acid)/$n$(GlcNAc) = 0.6–1.2), hydrolysis temperature (100–130 °C), and time (2–6 h). At the end of the hydrolysis reaction, double-stage centrifuge treatment was adopted to treat the NCh suspension. The acid collected from the first-stage centrifuge was further extracted and crystallized at low temperature for acid recovery and reused. The resultant NChs were dialyzed to remove the residual acid, followed by the second-stage centrifuge, which was fractionated into two types of products based on their interface stability. They are named ChNC and ChSR, respectively, and the corresponding structure, property, and potential application are evaluated below. The benefits of this novel method include the following:

(1) Green and sustainable hydrolysis with fully recyclable crystalline solid-type organic acid.

(2) Simultaneous production of two types of NCh products to minimize chitin loss.

(3) The process's high flexibility allows for the engineering of the resulting products and bridges the gap from process engineering to specific high-value applications.

## 3.2 Optimization of acid hydrolysis production

**Solid organic acid screening.** Different types of solid organic acids were examined for selective hydrolysis of chitin. The hydrolysis NCh product yields from different solid organic

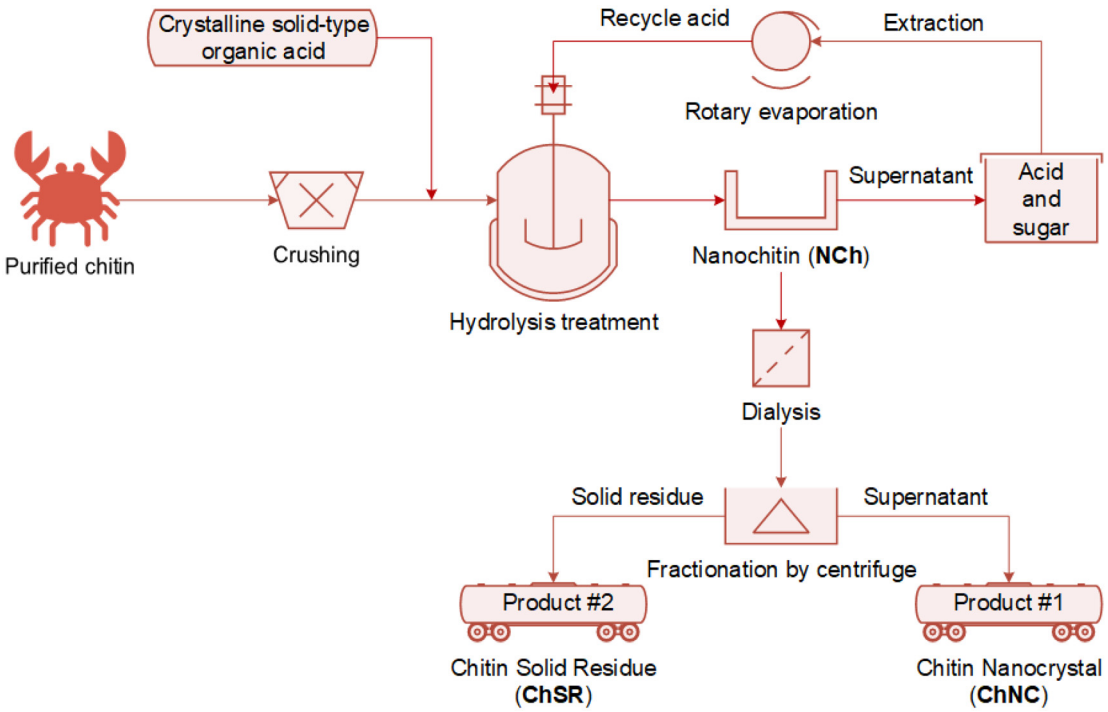


**Fig. 1** Schematic illustration of the preparation of two types of nanochitin products by a recyclable solid organic acid assisted hydrothermal treatment.

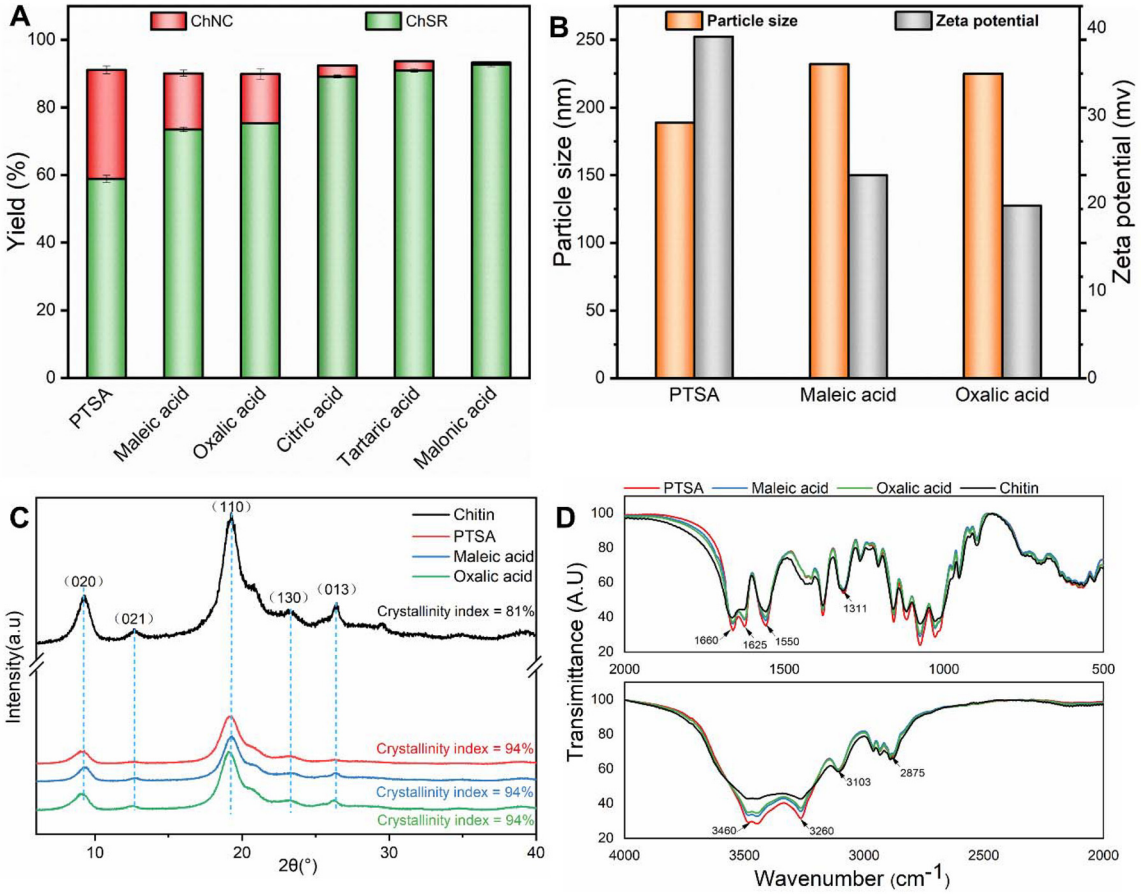


**Fig. 2** Effects of solid organic acid types on the yield of NCh products (A), the particle size and zeta potential (B), the crystallinity index (C) and the chemical structure (D) of the ChNC product; acid hydrolysis conditions: *n*(acid)/*n*(GlcNAc) = 1.2, 130 °C for 4 h under stirring of 200 rpm.

acids are shown in Fig. 2A. The total yield of NCh products from different acids is close to each other, whereas product distributions are heavily affected by the types of solid organic acids. Since the yield of solid products is as high as over 90%, only a small amount of water-soluble sugar products remains. The results indicate that all these solid organic acids react with chitin mainly *via* chain truncation to produce fragment products rather than end-wise depolymerization to produce water-soluble small molecules. The preference for the production of ChNC is higher in the order of PTSA > maleic acid > oxalic acid > citric acid > tartaric acid > malonic acid, which is consistent with the order of the p$K_a$ value of acids.[20] The further effect of organic acid types on the particle size and zeta potential of the ChNC product was then investigated. As shown in Fig. 2B, smaller chain truncation ChNC products are obtained from PTSA compared to that from maleic acid or oxalic acid, suggesting that a significant degree of chain truncation occurred during the acid hydrolysis or that the cleavage chitin fragments are more accessible to the PTSA. In agreement with the previous result that HCl-hydrolysed chitin nanocrystals exhibited positive charge,[21] as shown in Fig. 2B, PTSA produces more stable ChNC particles with higher positive zeta-potentials than malic acid and oxalic acid.

As presented in Fig. 2C, X-ray diffraction (XRD) patterns of the purified chitin and the corresponding NCh products exhibit identical four typical characteristic diffraction peaks of the α-chitin structure, located at $2\theta$ = 9°, 13°, 19°, 21° and 26.6°, which corresponded to the (020), (021), (110), (130), and (013) reflection planes, respectively.[22] It indicates that hydrolysis of all solid acids keeps the type of the original chitin crystal structure intact. The enhancement of the ChNC products' crystallinity index compared with the original chitin is attributed to the removal of the amorphous region of chitin. Notable, the crystallinity of all CHNC products by different types of acid hydrolysis processes is identical.

The FT-IR spectra of the ChNC products from different acid hydrolysis processes are compared in Fig. 2D. The characteristic peaks of purified chitin are observed at around 3460 $cm^{-1}$ (–OH stretching vibration), 3260 and 3103 $cm^{-1}$ (–$NH_2$ stretching), 2875 $cm^{-1}$ (–$CH_2$ and –$CH_3$ stretching), 1660 and 1625 $cm^{-1}$ (amide I band), 1550 $cm^{-1}$ (amide II bands), and 1311 $cm^{-1}$ (amide III bands).[23] The same characteristic bands corresponding to chitin are observed in these ChNC products, suggesting the elementary structure of chitin can be maintained for all hydrolysis treatments. However, the resonance of –OH and –$NH_2$ in the ChNC obtained by PTSA is stronger than

 

those two ChNC products obtained from maleic acid and oxalic acid. It indicates that PTSA is the most efficient in the cleavage of glycosidic and amide bonds among the organic acids investigated here.

Therefore, based on the above results of the yields, stability and structure of NCh products, PTSA is thus chosen for the catalytic hydrolysis of chitin to the NCh.

**Proposed mechanism and process of chitin hydrolysis.** Based on the previous literature,[19] a plausible mechanism for the hydrolysis of chitin catalyzed by PTSA is proposed in Fig. 3. PTSA is a strong organic acid ($pK_a = -2.8$) and thus can be easily ionized into protons in an aqueous solution. The attacking of these protons on the carbonyl group of the amide bond forms a hydroxyl group. Meanwhile, the carbon of the carbonyl group becomes more electrophilic and susceptible to addition with water molecules. Under the synergistic effect of protons and water, the amide bond of the GlcNAc molecules in chitin is broken, exposing protonated amino groups with a positive charge. As a result, the chitin chains become extremely swollen in water, facilitating the access of the PTSA molecules. The effective contact interaction between chitin and PTSA also contributes to the catalytic hydrolysis of chitin. There are two different interfacial driving forces of chitin and PTSA: one driving force can be attributed to strongly polarized hydrogen bonding between –OH and $–NH_2$ groups in chitin- and oxygen-containing functional groups in the PTSA; the second force can be ascribed to van der Waals forces between the hydrophobic C–H groups of chitins and hydrophobic aromatic regions in the PTSA. After contact with the surface of chitin sites, the cleavage of β-1,4-glycosidic bonds are executed by the strong $–SO_3H$ groups in the PTSA. The hydrolysis of chitin proceeds by the $–SO_3H$ groups *via* the internal breakage of the GlcNAc chain, finally resulting in more contact sites to accelerate the cleavage of chitin microfibrils into ChNCs mainly carrying $–NH_2$ groups and ChSRs mainly carrying acetyl groups. Moreover, this hydrolysis reaction can prevent the further conversion of chitin nanocrystals into water-soluble oligo-or mono-saccharides, considering the low yield of around 10% for the soluble products presented in the supernatant from first-stage centrifugation. Both of the above are responsible for the fact that the resulting stable NCh materials can be produced effectively over the PTSA catalysis.

**Statistical analysis, surface plots and optimization.** A 3-factor two-response central composite design (CCD) for response surface methodology (RSM) was used to investigate the correlation between the NCh product yields and process variables. The experimental design matrix and the responses based on 17 experimental runs conducted in our study are given in Table S1 of the ESI.† Based on the statistical analysis in the ESI,† all these statistical tests show that the quadratic models developed are qualified to represent the correlation

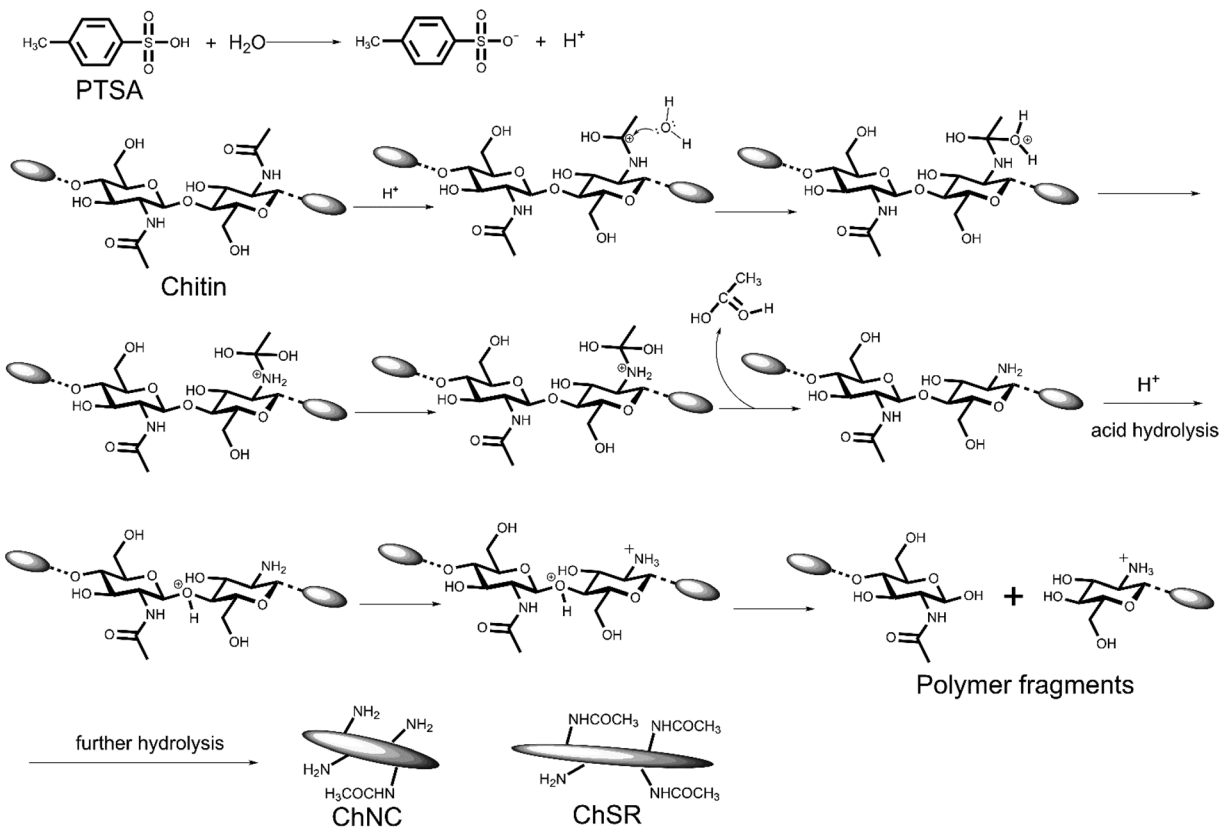


Fig. 3 Hydrolysis mechanism of chitin catalyzed over *p*-toluenesulfonic acid to produce two kinds of nanochitin products.

between the response and the independent process variables (Fig. S1 and Table S2 in the ESI†).

To better visualize the statistically significant factors derived from the statistical analysis, three-dimensional (3D) response surface plots and the corresponding contour plots are given in Fig. 4. These plots depict the combined effects of two factors on yields of NCh products, while another factor is kept constant at their medium levels. Under the same variation range, the response surface for ChNC yields show a convex shape, while that for ChSR yields show a concave shape. It can be explained by the fact that the ChNC is sequentially converted from ChSR by hydrolysis rather than directly obtained by one-step hydrolysis.

Fig. 4A and B show the interaction effects of acid molar ratio and reaction temperature on the yields of ChSR and ChNC, respectively. The shape of the contour plots is elliptical rather than circular, indicating that the mutual interactions between variables are significant in the chitin hydrolysis process. Generally, the loosely tangled amorphous region is more readily hydrolyzed than the compact ordered crystalline regions in chitin.[24] Consequently, most of the amorphous regions in chitin are degraded in the initial hydrolysis period, leaving the micro-sized chitin crystalline particles (ChNC) with a maximum amount. As shown in Fig. 4A, at any level of reaction temperature, the increase of acid molar ratio from 0.6 to 1.2 can slightly reduce the amount of ChSR. Accordingly, as shown in Fig. 4B, the ChNC yield from the hydrolysis of ChSR is only enhanced by around 12%. It indicates that independently increasing the acid concentration is limited in promoting the hydrolysis of the crystalline region to a smaller size. Meanwhile, the reaction temperature plays a crucial role in initiating and improving the chemical degradation of the chitin chain (from the microscale to the nanoscale). In the region of acid molar ratio of 0.6 (Fig. 4A), the amount of ChSR significantly decreases from 93% to 47% with the increased reaction temperature from 100 °C to 130 °C. As a result, in Fig. 4B, the ChNC yield is progressively increased from 3% to 45% at the reaction temperature of 100–130 °C. Similar trends are also observed at the high acid molar ratio (1.2) level for both ChSR and ChNC yields. On the one hand, the improved yield can be attributed to the energy barrier for breaking the hydrogen bonding system in chitin, which is lowered with increasing temperature. Consequently, the hydrolysing catalyst quickly penetrates and spreads evenly inside the individual crystallite segments, making the hydrolysis process more kinetically favorable.[25] On the other hand, the hydrolysis reaction rate is directly related to the temperature based on the thermal equilibrium theory:[26] the higher the temperature, the more the energy that is delivered to the reaction medium, resulting in easier cleavage of covalent bonds inside the chitin fragments (ChSR) and hence more chitin crystalline particles (ChNC) in nano-size are produced. Recent studies have supported this statement on preparing cellulose nanocrystals by using ionic liquids and $Ni(NO_3)_2$ catalysts.[26,27] The interaction effects of reaction temperature and time on ChSR and ChNC yields are displayed in Fig. 4C and D, respectively. It is observed from Fig. 4C that the yield of ChSR decreases with the increase of reaction temperature at a constant reaction time, especially when the reaction time is within the range of 2–6 h; the increase of reaction temperature from 100 °C to 130 °C leads to the reduction of ChSR content (96–47%). In contrast, the yield of ChNC shows an increasing trend with the increase of

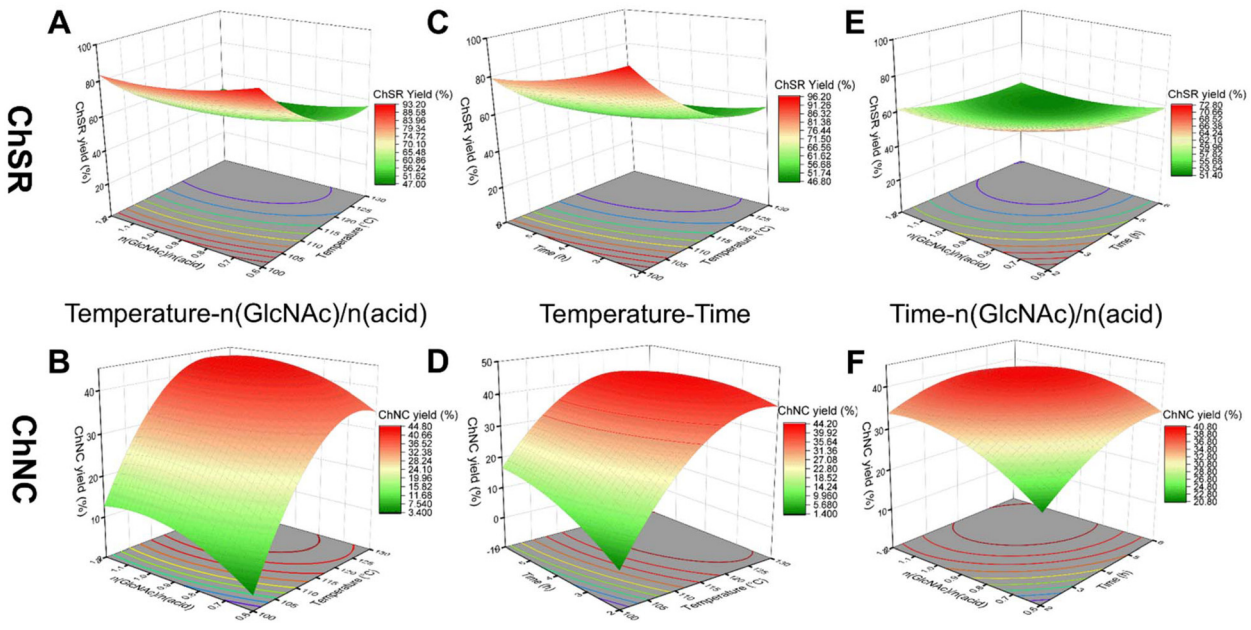


Fig. 4 Response surface and contour plots showing interaction effects of different process parameters on ChSR and ChNC yields: (A(B)) temperature × acid molar ratio; (C(D)) temperature × time; and (E(F)) time × acid molar ratio.

 

temperature, as shown in Fig. 4D; *e.g.*, at the low level of reaction time (2 h), the increase of reaction temperature from 100 °C to 130 °C leads to an increase of ChNC yield (1–44%). Also, the effects of reaction time show that the ChSR yield decreases from 96% to 80% with the reaction time increased from 2 h to 6 h when the hydrolysis temperature is 100 °C (Fig. 4C). An opposite trend can be observed in Fig. 4D, in which the ChNC yield gradually increases from 2% to 18%. It is noted that the contour plots for both ChSR and ChNC yields are elliptical, implying that the interactive effect of reaction temperature and time on yields is significant. High temperature is conducive to the diffusion of hydrolysing catalysts inside the chitin substrate, and the effect is accumulated with the progressive increment of contact time. Consequently, the surface area of treated chitin is increased due to the physical swelling phenomenon and the disintegration of the glycosidic linkage of chitin fibres initiated until its maximum level. An increment in temperature results in an enhanced hydrolysis rate and shortens the reaction time to achieve a high yield of ChNC. However, excessive heat energy causes the color of solid products to deepen and even over-degrades solid products to the water-soluble by-products. The simultaneous dependence of ChSR and ChNC yields on the time *vs.* acid molar ratio is shown in Fig. 4E and F, respectively. Their corresponding contour plots are close to circular, indicating the relatively mild interactive effects of the two independent variables on the yield. Based on the above results, our hydrolytic reaction to effectively produce high crystalline NCh should be restricted to a shorter time and be more manageable under normal atmospheric pressure conditions.

Finally, the optimal conditions to obtain the maximum yield of ChNC and ChSR are predicted as follows: $n$(acid)/$n$(GlcNAc) = 1.2, reaction temperature = 130 °C, reaction time = 6 h. Under the optimal conditions, as shown in Table 1, the experimental yield of ChNC is 39%, and that of ChSR is 54%, which is not significantly different from the predicted values of 41% and 53% at a 95% confidence interval, respectively. In the hydrodynamic diameter distribution pattern measured by dynamic light scattering, the obtained ChSR has an average diameter of about 169 nm with a relatively broad size distribution (PDI = 0.8). In contrast, the ChNC, with an average diameter of about 50 nm, was further degraded from ChSR. Moreover, the ChNC particles have a uniform architecture with a PDI value of 0.3. In addition, the zeta-potential results indicate that ChNC has better colloidal stability than ChSR. It further confirms that chitin chains deacetylated to form cationic NChs as the hydrolysis progressed. Therefore, the model helps to predict the optimal acid hydrolysis process parameters for producing different types of NChs.

**Table 1** Evaluation of the yields and properties of ChNC and ChSR under optimum conditions

| | Predicted yield (%) | Experimental yield (%) | *Z*-average size (nm) | PDI | Zeta potential (mV) |
|---|---|---|---|---|---|
| ChSR | 53 | 54 | 169 | 0.8 | +35 |
| ChNC | 41 | 39 | 50 | 0.3 | +41 |
| Total | 94 | 93 | — | — | — |

**Recycle and reuse of PTSA.** The cycling stability of PTSA in hydrolysis waste was evaluated to develop a cost-effective hydrolysis technology. Due to the high solubility in ethyl acetate and low solubility in water for PTSA, substantial PTSA was recovered from hydrolysates by simple extraction and recrystallization processes. Fig. S2 and S3 in the ESI† show the NMR spectra of the original and recycled PTSA (R-PTSA), which can verify the structure integrity of PTSA after recovery. The recovery yield and purity of R-PTSA are presented in Table S3 of the ESI.† The theoretical recovery of R-PTSA as a catalysis almost remained at 100%, whereas the actual recovery yield of R-PTSA is 80%. Meanwhile, the obtained R-PTSA has a high purity of 90%, approaching commercial PTSA's purity. The difference between the theoretical and actual recovery can be explained by the fact that part of the PTSA remained in the supernatant of the hydrolysis suspension and the mother liquid of recrystallization. The reuse of the R-PTSA for NCh production was studied, and the results are compared with the original PTSA in Table S3.† It is found that the hydrodynamic diameter distribution and zeta-potential of ChNC obtained from the recycling experiment are close to those obtained from the original experiment. Moreover, the PTSA can be used repeatedly without significantly losing its catalytic activity, and the yield of NCh is almost at the same high level.

### 3.3 Verification of NCh production from crustacean shell waste

Next, we performed scale-up production of NChs from three species of crustacean biomass in one-pot modified from the above optimal conditions (as shown in Fig. 5A). The results in Fig. 5B illustrate that different biomass have different composition. Their chitin contents are close to each other, whereas the mineral content is the highest in the crab and the protein content is the highest in the shrimp. The $CaCO_3$ minerals of crustacean samples are well exposed and accessible at the surface due to the milling procedure. This is desirable as it facilitates the demineralization by PTSA with the formation of $CO_2$. After foam evolution ceased, additional PTSA was added to start the deproteinization and chitin hydrolysis reaction with heating and stirring. It is generally accepted that protons and hydroxide generated in hydrothermal water can promote acid- and base-catalysed hydrolysis of proteins into peptides, amino acids and ammonia.[28–30] Thus, we consider subcritical water sufficient to decompose proteins from these crustacean samples and leave the chitin to be hydrolysed into nanoparticles under PTSA catalysis. In Fig. 5B, the overall mass yield of NChs is 59% from crab (abbreviated as $NCh_{crab}$) and 96% from crawfish based on the chitin available in biomass. The over-hydrolysis of chitin in crabs can be attributed to a high amount of easily degradable $CaCO_3$ and a low amount of inert protein under acidic conditions. For the same reason, over 100% of NChs is obtained from shrimp due to the high amount of protein. Therefore, the production of NChs with our system is more effective for crustacean biomass, which is

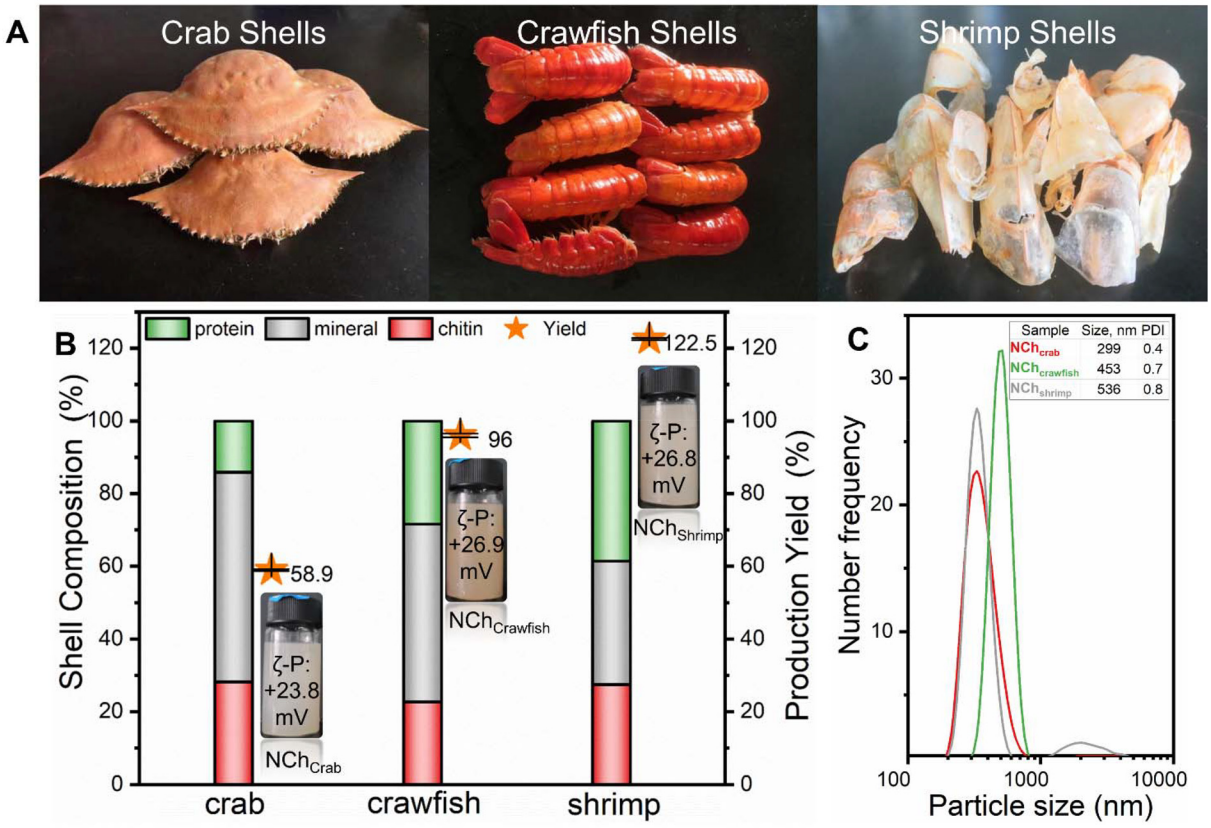


**Fig. 5** Large-scale preparation of NChs directly from Crustacean biomass waste: (A) image of the raw materials; (B) composition of the raw materials and information of their corresponding nanochitin products; and (C) the particle size distribution of nanochitin products.

rich in minerals than protein. Also, all the NChs carrying a positive charge (zeta-potential = +24–27 mV) straight from Crustacean biomass could be colloidally stable in water. Fig. 5C shows the hydrodynamic diameter distribution results of the NCh. The average size was 299, 453, and 536 nm for $NCh_{crab}$, $NCh_{crawfish}$, and $NCh_{shrimp}$, respectively. Moreover, the chitins in the crab shell were sufficiently hydrolyzed into the $NCh_{crab}$ with a PDI value of 0.4. In contrast, the chitins in the shrimp shell were insufficiently hydrolyzed into the $NCh_{shrimp}$, resulting in an uneven particle distribution (PDI = 0.8). Therefore, these tests suggest that the crab shell is the best crustacean biomass waste for scalable production of NCh.

### 3.4 Characterization of the NCh products

**Morphological and structural properties.** The morphologies and dimension distribution of ChSR, ChNC, and $NCh_{crab}$ are shown in Fig. 6. Their TEM and AFM images exhibit a considerably similar short rod-like morphology with a short length and small aspect ratio. Moreover, the resultant nanoparticles' dimensions depend on the severity of the hydrolysis. As shown in Fig. 6A, the ChSR shows bundled nanocrystals with an average height of approximately 26 nm. Furthermore, ChSR has a long length ranging from 100 nm to 450 nm, and its width mainly ranges from 10 nm to 30 nm. Thus, the aspect ratio of ChSR exhibits a broad distribution ranging from 10 to 15. In contrast, the PTSA precisely fractures β-1,4-glycosidic bonds and continuously cut the amorphous regions inside the chitin nanofibrils, resulting in a narrow distribution of ChNC dimensions, as shown in Fig. 6B. The ChNC possesses a length and width range of 25–225 nm and 15–30 nm, respectively, and the aspect ratio of ChNC only ranges from 2 to 8. The single or individual nanocrystals with an average height of approximately 9 nm are typical in the ChNC samples. In addition, acidic hydrothermal treatment substantially facilitates the scalable production of NCh straight from crustacean biomass, and the as-prepared $NCh_{crab}$ has an average height of approximately 40 nm without fractionation, as exhibited in Fig. 6C. Besides, $NCh_{crab}$ has a width ranging from 20 nm to 50 nm, and their length primarily ranges from 200 nm to 700 nm. Therefore, the aspect ratio of $NCh_{crab}$ exhibits a similar distribution as ChSR from 10 to 14. It indicates that the morphological properties of one-pot prepared $NCh_{crab}$ are already perfect compared with that of ChSR prepared from purified chitin, and further hydrolysis is necessary to reach the properties of ChNC.

The XRD patterns of three types of NCh products are shown in Fig. 7A. The $NCh_{crab}$ exhibits a similar crystal structure and crystallinity index compared with the other two kinds of NCh products from purified chitin. The crystallinity of ChNC (84%) is slightly lower than that of ChSR (89%), which can be attribu-

 

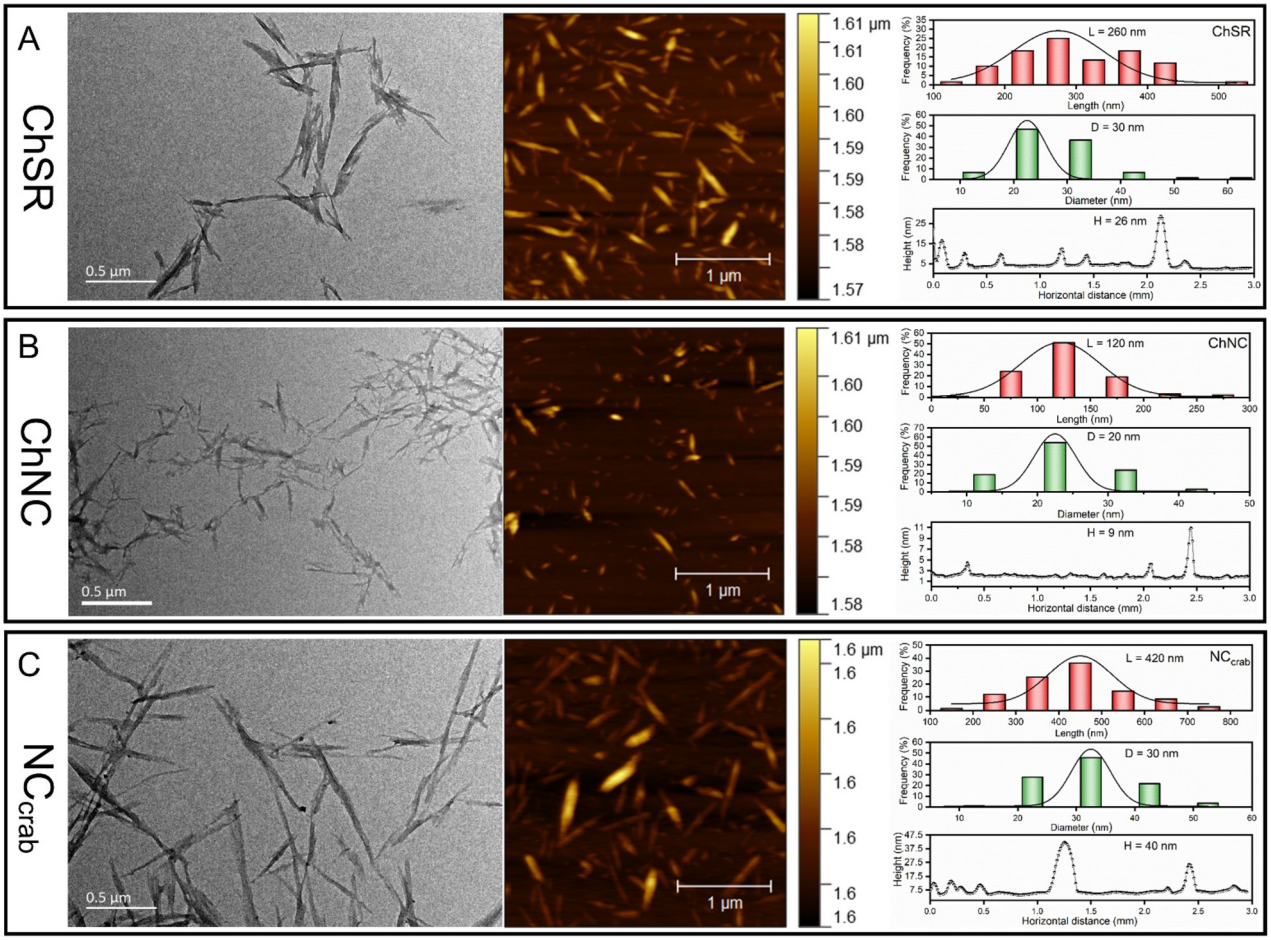


**Fig. 6** Morphology of the nanochitin products obtained under the optimal conditions: TEM and AFM images and size distributions of ChSR (A), ChNC (B) and $NCh_{crab}$ (C).

ted to the partial destruction of the crystalline structure and results in more disordered regions in chitin nanofibrils caused by further hydrolysis.[31] As a result, the increased effective surface area of chitin improves the accessibility of PTSA reagents to the amide bonds and led to a high charge content.

The FT-IR spectroscopy was used to investigate the chitin's chemical structure evolution during acid hydrolysis (Fig. 7B). However, since the difference between spectra of ChSR and ChNC are subtle, their structural difference is hardly distinguished. In addition, the $NCh_{crab}$ with a typical chitin's infrared structure spectrum indicates that the extraction and preparation of NCh from crustacean biomass waste can be realized in one-pot by our hydrolysis system.

The solid-state cross-polarization magic angle spinning carbon-13 nuclear magnetic resonance ($^{13}C$ CP/MAS-NMR) technique was thus employed to get more detailed information on NCh products (Fig. 7C). Their $^{13}C$ NMR spectra show eight well-defined resonances of C1–C6 and acetyl, which are $\varepsilon$ = 174 ppm for the C═O bond, $\varepsilon$ = 103 ppm for C1, $\varepsilon$ = 83 ppm for C4, $\varepsilon$ = 75 ppm for C5, $\varepsilon$ = 61 ppm for C6, $\varepsilon$ = 56 ppm for C2, and $\varepsilon$ = 23 ppm for $CH_3$.[32] The original chitin and the corresponding ChSR and ChNC products are pure and contain no other impurity, as indicated by the peaks differing from their spectra at a very low level. The degree of acetylation (%DA) was calculated by measuring relative integrals of a methyl group ($CH_3$) compared to the carbon integrals of the polysaccharidic backbone (Fig. S4–S6†).[33] The %DA was 99% for original chitin and gradually decreases as the hydrolysis progress. Specifically, the ChSR product exhibits 96%DA, just slightly lower than that for chitin, whereas the %DA of the ChNC product was found to be 90% (Fig. 7C). These results confirm that the breaking of the NH–C(O) bond occurs during the PTSA hydrolysis and that the ChNC is the further deacetylated product of ChSR.

The thermogravimetric (TG) and derivative thermogravimetric (DTG) curves of chitin and NCh products hydrolyzed by PTSA are presented in Fig. 7D. All samples show three distinctive steps of thermal degradation in the TG curves. In the first stage, a weight loss rate of *ca.* 2–8% happens below 100 °C due to the removal of adsorbed water and volatile components upon heating.[34] In the second stage, a sharp weight loss rate is observed from 200 to 400 °C, mainly caused by the

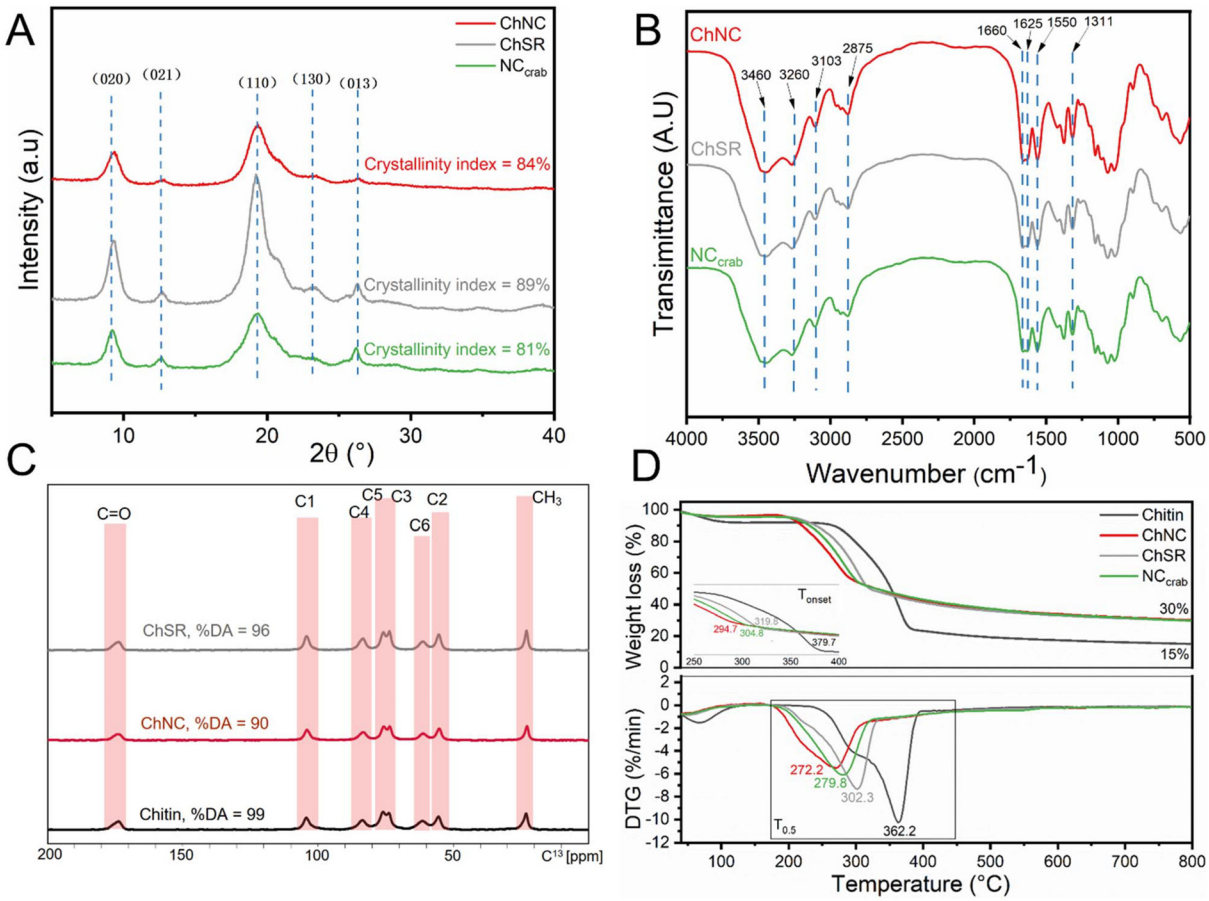


Fig. 7 XRD patterns (A), FT-IR spectra (B), $^{13}C$ solid-NMR spectra (C), and TG and DTG curves (D) of NCh products.

chitin degradation due to the depolymerization, dehydration, or decomposition of the glycosyl unit, followed by the formation of charred residue.[35] Both the starting decomposition temperature ($T_{onset}$) and mid-point of the decomposition temperature ($T_{0.5}$) of the samples are higher in the order of ChNC < $NCh_{crab}$ < ChSR < chitin, as shown in the TG and DTG curves. In contrast with the original purified chitin, the decrease in the thermal degradation of the corresponding NCh products is due to the conversion of chitins to nano-elements, benefiting the amounts of chitin crystallite surfaces and the heat transfer rate.[36,37] The thermal stability of nano-scale chitin particles also decreased, as reported in the previous studies.[34,37,38] The difference in thermal stability among NCh products appeared to relate with the purity, particle size, crystallinity, and DA%. The NMR spectra of NCh products show that the ChNC and ChSR are pure, whereas the $NCh_{crab}$ directly extracted from crustacean waste contains protein-related impurities (see Fig. S7 in the ESI†). Considering that the impurity derivatives in the $NCh_{crab}$ could significantly affect its thermal stability, we will not give further comparison discussion on $NCh_{crab}$. For the clean NCh products originating from purified chitin, it is reasonable that the obtained ChNC with a smaller size and lower crystallinity by further PTSA hydrolysis shows a decrease of thermal stability compared with that of obtained ChSR. Also, the reported negative relationship between thermal stability and degree of deacetylation for chitin/chitosan nanofibers agrees with our results in Fig. 7C and D.[39] In the last stage of 400–800 °C, the slight weight loss is ascribed to the further depolymerization of residual char into volatile products.[33] The final amount of char residues at 800 °C for NCh products (30%) is noticeably larger than that for chitin (15%). A reasonable explanation for this can be referred to the research on similar nanomaterials, like cellulose nanocrystals.[40,41] The number of free-end chains on the surface of chitin increases significantly as its size reduces to a nanometer scale. These end chains quickly decompose at lower temperatures, consequently facilitating the increase of char residue.

**Self-assembly and interfacial behavior.** The self-assembly and interfacial behavior of NCh products is essential for their application in three-dimensional structural nanomaterials. Due to the sufficient dispersibility and stability of ChNC aqueous dispersion, the self-assembly periodic nanostructures can be generated in the solid state by evaporating the ChNC suspensions, giving rise to yellow transparent film (Fig. 8A). The cross-sectional SEM image (Fig. 8A) shows a highly ordered hierarchical architecture analogous to that

 

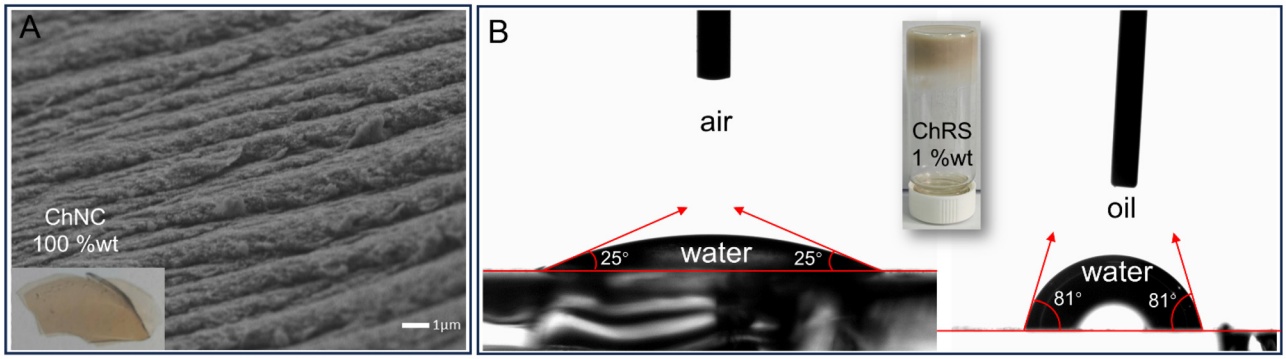


**Fig. 8** Assembly and interfacial behavior of the NCh products: ChNC (A) and ChSR (B).

found in nature or artificial composites. Therefore, our produced ChNC can be used as periodically nanostructured thin-film interference filters to alter the dispersion relationship of photons.[14] In terms of the ChSR product, as imaged in Fig. 8B, a significant aspect ratio makes it gel-like at low concentrations. Due to the amphiphilic nature of the ChSR particle, its water contact angles in the air phase ($\theta_{aw}$) and oil phase ($\theta_{ow}$) were determined. As shown in Fig. 8B, ChSR particles produce a $\theta_{aw}$ value of *ca.* 25° and $\theta_{ow}$ value of *ca.* 81° (measured after 120 s). The ChSR particles have good surface wetting, suggesting an abundance of –OH and $-NH_2$ groups exposed on their surface. In addition, according to the theory and assuming a single interfacial layer,[42,43] the ChSR particles with $\theta_{ow}$ between 15° and 90° are effective in stabilizing O/W Pickering emulsions. Moreover, the macroscopic viscosity enhanced by the formation of the 3D network could give them an extra advantage for the application of emulsion stabilization.[44]

### 3.5 Application examples of NCh

The nanocelluloses and nanochitins are examples of some of the most promising biobased nanoparticles. The assembly of nanocelluloses has been the subject of widespread studies, which shows great potential application in composite molding, controlled photonics, delivery systems, and catalyst preparation.[45–48] However, the single type of functional group distribution on the surface of nanocelluloses does not have natural advantages in their assembly; thus, introducing charged or hydrophobic groups on the surface of nanocelluloses is necessary to realize their assembly with efficient and precise control. For instance, a stable aqueous suspension of cellulose nanocrystals (CNCs) with thixotropic gelling properties and a shear birefringence phenomenon was obtained by grafting the ammonium-containing groups onto the CNC surface;[49] amphiphilic CNCs were produced to be used as a stabilizer in soybean oil/water emulsions by introducing lipophilic groups. Compared with the unmodified CNCs, an apparent effect of the lipophilic groups in the amphiphilic CNCs was observed as the emulsion droplet sizes decreased by a decade.[50] Notably, the NCh itself bears a positively charged and amphiphilic nature after the acid hydrolysis treatment since surface protonated amines structurally originate from the deacetylation of acetylglucosamine, and the rest of acetyls expose the hydrophobic planes.[9,51] Therefore, we envision that these NCh materials with positive charge or amphiphilic nature will open a sustainable avenue in the fabrication of photonic film or stable Pickering emulsion.

**Fabrication of photonic film with ChNC.** Structural coloration is a nature-inspired phenomenon that produces colors through the interference of light scattered by intrinsic nano- or micro-structures.[52] The corresponding materials have been extensively employed in many fields, including display, sensing, anti-counterfeiting, actuators, *etc.*[52–54] Even though the self-assembly periodic nanostructures of NCh materials driven by water-evaporation have been reported to enable potential optical applications at a small scale,[14,55] the lack of scalable methodologies to produce large-area colored films challenge their commercial exploitation. Herein, as shown in Fig. 9A, we overcome this limitation and demonstrate an industrially relevant route to scale up the production of photonic film by spraying our produced ChNC suspension on commercial stainless-steel plates (10 cm in length and width). Through optimization of the spraying parameters affecting the self-assembly process (Fig. S8†), we fabricated a photonic film with iridescent colors across the entire visible spectrum. This color construction approach shows excellent potential in fantastic automobile painting, as exemplified in Fig. 9B. A stainless-steel plate (10 mm in length and width) was selected as the representative to study the mechanism of structural color generation. As shown in Fig. 9C, the color of the photonic film sprayed onto the plate finally turns to red-green-yellow of the completely evaporated structure. In the POM photos (Fig. 9D), a local lamellar ordering of ChNC can be observed in the photonic film. It appeared that the interference color pattern is related to the layered ordering of the nanocrystal by the self-assembly process. The organization of the ChNC into a stable layered structure during the spraying and evaporation process is critical for forming macroassembled ChNC architecture with a tuned structure and ordered morphology. PVA has excellent film-forming and adhesive properties and is often used as a dispersant and stabilizer in various coatings and 3D printing.[56] Accordingly, the ChNC are dispersed in the PVA solution

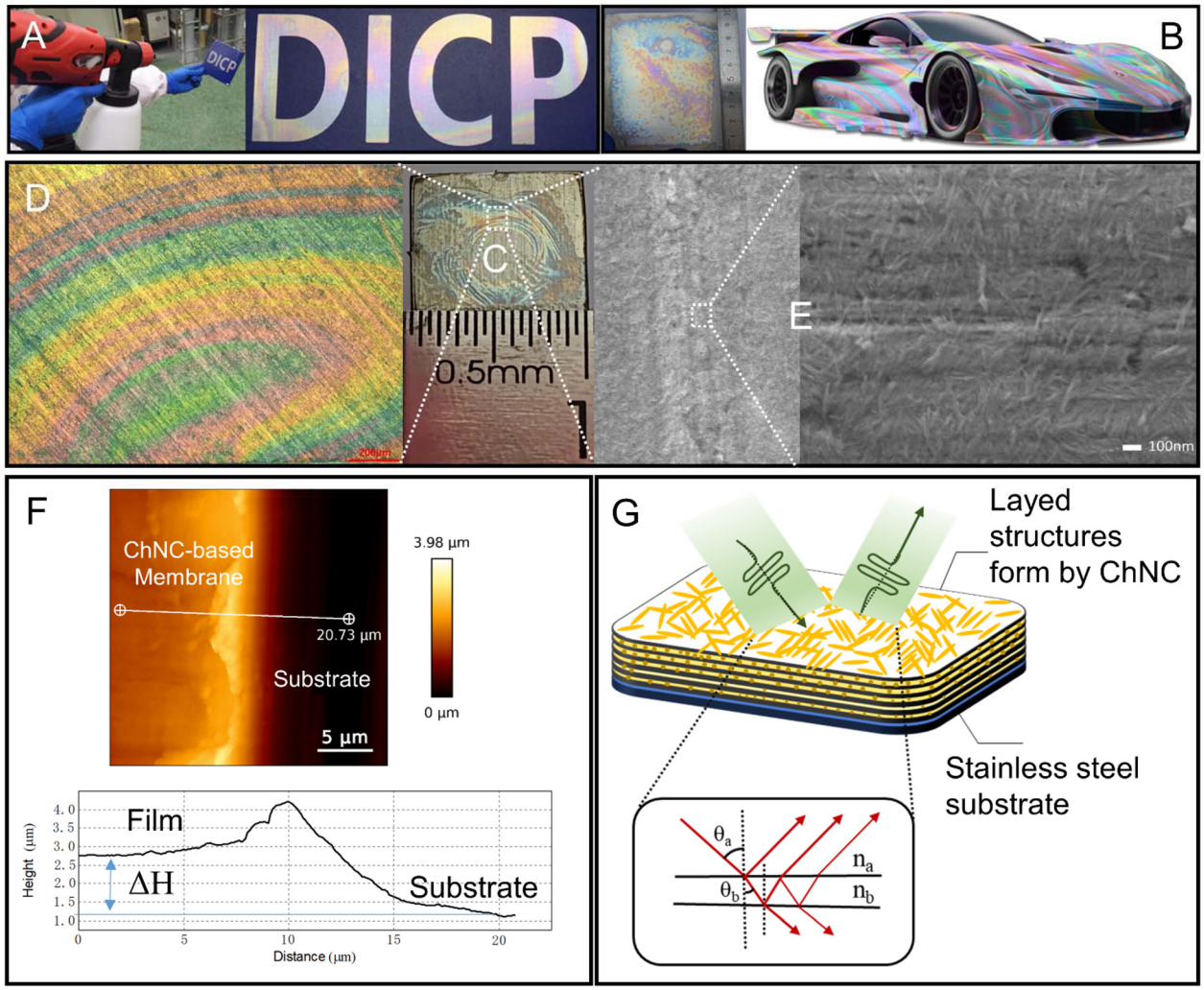


**Fig. 9** Application of ChNC in the preparation of photonic films. (A) Image of the spraying on-site; (B) image of the photonic film sprayed onto the commercial stainless-steel plates (10 cm in length and width) and an example of automobile painting; (C) image of the photonic film sprayed onto the commercial stainless-steel plates (10 mm in length and width); POM image (D) and SEM images (E) of the photonic film; (F) example of the AFM plane morphology of the photonic film, and the bottom height *vs.* distance image of the corresponding section profile along the white line; and (G) the thin film diffraction diagram.

to fabricate a structural color paint, on which the occurrence of the surface $-NH_2$ and $-NHCOCH_3$ groups functions to realize the stable distribution of particles inside the PVA polymer skeleton even for the wholly evaporated structure. It can be ascribed to the formation of strong hydrogen bonds between the $-NH_2$/$-NHCOCH_3$ groups of ChNC and the –OH groups of PVA, resulting in the stable dispersion of nanocrystal particles inside the sprayed microdroplet and the structural ordering preservation at the final stages of water loss from the droplet. As shown in Fig. 9E, the distribution of nanocrystal particles and PVA polymer skeleton after evaporation are characterized by SEM. From the surface SEM image, a uniform and ordered multilayered structure was observed; the enlarged SEM image demonstrates that the ChNC particles form a close-packed arrangement, and the PVA polymer chains uniformly intersperse the gaps among them on all side surfaces. In order to accurately characterize the thickness of the film, we created a zone consisting of the substrate and undamaged film to be measured by high-resolution AFM, as shown in Fig. 9F. The white profile and the related height *vs.* distance relationship provide that the thickness of the photonic film is 1.4 μm. It is an average value of 5 datasets measured in different places (Fig. S9†). Consequently, when light waves travel through a system of periodically modulated indices, they are reflected by the upper and lower boundaries of this thin film and interfere with one another,[57] finally generating a bright and vivid structural color (Fig. 9G).

**Production of Pickering emulsion gels with ChSR.** Replacement of synthetic surfactants derived from unsustainable fossil resources with sustainable and green biomass-based particles in the formulation of foodstuff-related emulsions is of great importance.[58,59] These particles can form an interfacial

 

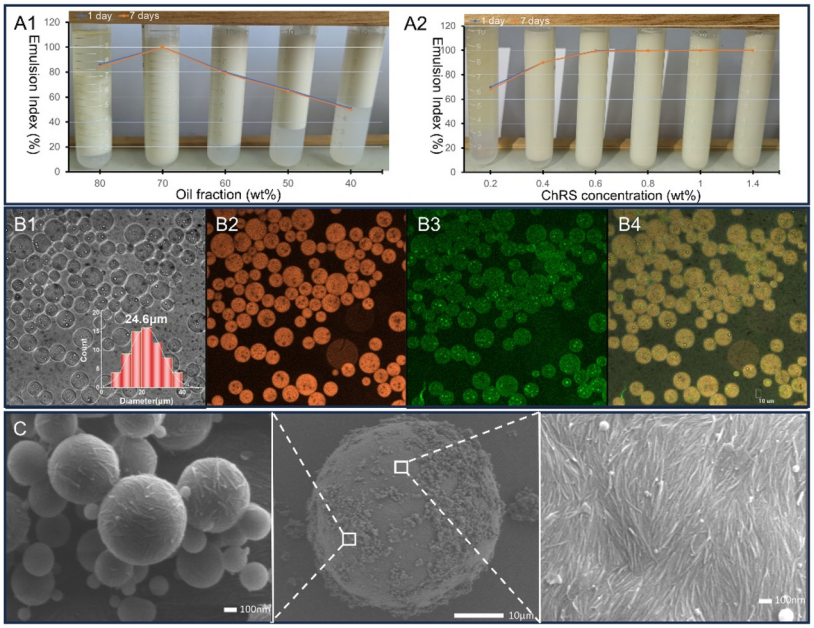


**Fig. 10** Application of ChSR in the preparation of the Pickering emulsion. (A) The effect of oil fraction and ChSR concentration on the stability of the soybean oil emulsion; (B) fluorescence micrographs of emulsion droplets stabilized by using an oil-to-water ratio of 7/3, and the 1.0 wt% ChSR; and (C) the SEM images of polymerized styrene-in-water emulsions stabilized by ChSR.

layer to prevent coalescence, increasing the kinetic stability of the emulsions. It is speculated that amphiphilic ChSR particles can perform similarly. Therefore, it is of interest to test the performance of ChSR solids in this application. The performance of ChSR in stabilizing the soybean oil emulsion was evaluated and optimized by visual inspection with the corresponding emulsion index shown in Fig. 10A1 and A2. The Pickering emulsion fabricated with the ChSR suspension at an oil fraction of 70 wt% shows high stability against creaming and oiling-off after storing at room temperature for seven days (Fig. 10A1). The milk-like emulsions consisting of ChSR with concentrations higher than 0.6 wt% are relatively homogeneous, and no excess oil was observed at the bottom of the emulsion after storing at room temperature for seven days (Fig. 10A2). It suggests that ChSR at a low concentration is insufficient to protect the coalescence of the oil droplets, resulting in sedimentation of the large emulsion droplets with stabilizing particles. The statistical droplet size distribution of the emulsions upon preparation and after being deposited at room temperature for seven days is illustrated in Fig. S10 and S11,† which further validates the optimal results on emulsion stability. The location of soybean oil and ChSR in the emulsion was further investigated by multichannel fluorescent microscopy. Under the bright field (Fig. 10B1), all droplets within the optimized emulsion appear spherical with an average diameter of 24.6 μm, following a standard distribution model. The red-colored soybean oil droplets are isolated and surrounded by the aqueous continuous phase of green-colored ChSR, confirming the O/W emulsion type (Fig. 10B2 and B3). The green halo covering the edge of the red oil droplets, shown in the merged images of Fig. 10B4, provides direct evidence of a typical Pickering stabilizing mechanism.[60,61] It is also confirmed by the reference system, in which styrene in-water emulsions are stabilized with the ChSR and polymerized into solid beads.[31,62,63] SEM images of PS beads (Fig. 10C) show that ChSR fibral particles are identically evenly distributed on the surface and curved along the droplets, building an armored layer. Moreover, a loose-networked organization of tiny droplets is distributed on the surface of large droplets, and the free dispersed ChSR interconnects them. Therefore, the stabilization of the emulsion droplet takes place through irreversible adsorption of ChSR fibril particles at the surface of the emulsion droplet and is subsequently interconnected by the rest of the dispersed ChSR, which lead to increased viscosity and thus prevents the accumulation of emulsion droplets.

## 4 Conclusions

A simple, environmentally friendly, and flexible shell biorefinery process for integrated utilization of all NCh products in high-value applications has been suggested. It consists of a PTSA-assisted-hydrothermal treatment followed by centrifugal fractionation of NChs from the resulting suspension, thus resulting in ChNC and ChSR products. Under the optimum conditions predicted by the response surface methodology (molar ratio of PTSA to GlcMAc units in chitin of 1.2, 130 °C, 6 h), a ChNC production yield of 39% with simultaneous 54% recovery of ChSR product to achieve minimum chitin loss was obtained. A high quantity of NChs was also produced under the modified optimal conditions directly from crustacean

shells by using hot water for deproteinization, PTSA for demineralization, and deliberation of chitin microfibrils. The ChSR product was bundled nanocrystals with a long length ranging from 100 nm to 450 nm and a width mainly ranging from 10 nm to 30 nm. Due to the ChSR particle's amphiphilic nature, it had an excellent interfacial behavior between water and oil phases. In contrast, the further hydrolyzed individual nanocrystal products (ChNC) with a length and width range of 25–225 nm and 15–30 nm, respectively and a high zeta-potential of 41 mV showed a self-assembly behavior to form a highly ordered hierarchical architecture, owing to abundant $-NH_2$ groups distributed on its surface. Accordingly, examples of high-value applications of ChNC products in fabricating large-area photonic films and ChSR products in stabilizing Pickering emulsion were last reported.

## Data availability

The data supporting this article have been included as part of the ESI.†

## Conflicts of interest

The authors declare no competing financial interest.

## Acknowledgements

This work was supported by the National Natural Science Foundation of China (grant 22108273 to X. Z.) and the Youth Innovation Fund of Dalian Institute of Chemical Physics (DICP I202132 to R. L.). We gratefully acknowledge the help from Prof. Guang Chu at Southeast University for the discussion on the structural color.

## References

1 Biomass explained-U.S. Energy Information Administration (EIA), **https://www.eia.gov**, retrieved 2024-05-24.
2 F. M. Kerton, Y. Liu, K. W. Omari and K. Hawboldt, *Green Chem.*, 2013, **15**, 860–871.
3 L. Carlsen and R. Bruggemann, *Int. J. Sustain. Dev. World Ecol.*, 2021, **29**, 219–229.
4 X. Chen, H. Yang and N. Yan, *Chem. – Eur. J.*, 2016, **22**, 13402–13421.
5 N. Yan and X. Chen, *Nature*, 2015, **524**, 155–157.
6 H. Sashiwa and S. Aiba, *Polym. Sci.*, 2004, **29**, 887–908.
7 T. Philibert, B. Lee and N. Fabien, *Appl. Biochem. Biotechnol.*, 2017, **181**, 1314–1337.
8 L. Bai, L. Liu, M. Esquivel, B. L. Tardy, S. Huan, X. Niu, S. Liu, G. Yang, Y. Fan and O. J. Rojas, *Chem. Rev.*, 2022, **122**, 11604–11674.
9 L. Bai, T. Kamarainen, W. Xiang, J. Majoinen, J. Seitsone, R. Grande, S. Huan, L. Liu, Y. Fan and O. J. Rojas, *ACS Nano*, 2020, **14**, 6921–6930.
10 Y. Fan, T. Saito and A. Isogai, *Biomacromolecules*, 2008, **9**, 192–198.
11 L. Liu, L. Bai, A. Tripathi, J. Yu, Z. Wang, M. Borghei, Y. Fan and O. J. Rojas, *ACS Nano*, 2019, **13**, 2927–2935.
12 Y. Fan, T. Saito and A. Isogai, *Biomacromolecules*, 2008, **9**, 1919–1923.
13 K. G. Nair and A. Dufresne, *Biomacromolecules*, 2003, **4**, 657–665.
14 A. Narkevicius, L. M. Steiner, R. M. Parker, Y. Ogawa, B. FrkaPetesic and S. Vignolini, *Biomacromolecules*, 2019, **20**, 2830–2838.
15 L. Chen, J. Y. Zhu, C. Baez, P. Kitin and T. Elder, *Green Chem.*, 2016, **18**, 3835–3843.
16 H. Yang, G. Gözaydın, R. R. Nasaruddin, J. R. G. Har, X. Chen, X. Wang and N. Yan, *ACS Sustainable Chem. Eng.*, 2019, **7**, 5532–5542.
17 J. L. Shamshina and N. Abidi, *ACS Sustainable Chem. Eng.*, 2022, **10**, 11846–11855.
18 J. Jiang, Y. Zhu and F. Jiang, *Carbohydr. Polym.*, 2021, **267**, 118188.
19 W. Yang, J. Wang, L. Jiao, Y. Song, C. Li and C. Hu, *Green Chem.*, 2022, **24**, 1362–1372.
20 D. D. Perrin, B. Dempsey and E. P. Serjeant, *pKa prediction for organic acids and bases*, 1981.
21 Y. Fan, H. Fukuzumi, T. Saito and A. Isogai, *Int. J. Biol. Macromol.*, 2012, **50**, 69–76.
22 W. T. Wang, J. Zhu, X. L. Wang, Y. Huang and Y. Z. Wang, *J. Macromol. Sci., Part B: Phys.*, 2010, **49**, 528–541.
23 S. Cao, W. Gu, W. Ou-Yang, D. Chen, B. Yang, L. Lai, Y. Wu, Y. Liu, J. Zhu, W. Chen, Z. Gai, X. Hou, Y. Ma and Y. An, *Carbohydr. Polym.*, 2019, **213**, 304–310.
24 J. D. Goodrich and W. T. Winter, *Biomacromolecules*, 2007, **8**, 252–257.
25 C. W. Shuai, Y. H. Peng, L. Y. Xing, C. P. Chen, Z. M. Xin and H. Y. Fei, *Carbohydr. Polym.*, 2011, **83**, 1804–1811.
26 M. Yahya, Y. W. Chen, H. V. Lee, C. C. Hock and W. H. W. Hassan, *J. Polym. Environ.*, 2019, **27**, 678–702.
27 X. Y. Tan, S. B. A. Hamid and C. W. Lai, *Biomass Bioenergy*, 2015, **81**, 584–591.
28 O. Tavakoli and H. Yoshida, *Green Chem.*, 2006, **8**, 100–106.
29 T. M. Aida, M. Oshima and R. L. Smith Jr, *ACS Sustainable Chem. Eng.*, 2017, **5**, 7709–7715.
30 I. Marcet, C. Álvarez, B. Paredes and M. Díaz, *Waste Manage.*, 2016, **49**, 364–371.
31 P. R. Chang, R. Jian, J. Yu and X. Ma, *Carbohydr. Polym.*, 2010, **80**, 420–425.
32 J. L. Shamshina, R. S. Stein and N. Abidi, *Green Chem.*, 2021, **23**, 9646–9657.
33 R. M. Abdel-Rahman, R. Hrdina, A. M. Abdel-Mohsen, M. M. Fouda, A. Y. Soliman, F. K. Mohamed and T. D. Pinto, *Int. J. Biol. Macromol.*, 2015, **80**, 107–120.
34 A. A. Oun and J. W. Rhim, *Carbohydr. Polym.*, 2017, **175**, 712–720.

 

35 S. Shankar, J. P. Reddy, J. W. Rhim and H. Y. Kim, *Carbohydr. Polym.*, 2015, **117**, 468–475.
36 F. Jiang and Y. L. Hsieh, *Carbohydr. Polym.*, 2013, **95**, 32–40.
37 Y. Fan, H. Fukuzumi, T. Saito and A. Isogai, *Int. J. Biol. Macromol.*, 2012, **50**, 69–76.
38 J. L. Shamshina and N. Abidi, *ACS Sustainable Chem. Eng.*, 2022, **10**, 11846–11855.
39 Y. S. Nam, W. H. Park, D. Ihm and S. M. Hudson, *Carbohydr. Polym.*, 2010, **80**, 291–295.
40 N. Wang, E. Ding and R. Cheng, *Polymer*, 2007, **48**, 3486–3493.
41 Q. Liu, N. Chen, X. Yin, L. Long, X. Hou, J. Zhao and X. Yuan, *Int. J. Biol. Macromol.*, 2021, **181**, 621–630.
42 B. P. Binks, *Curr. Opin. Colloid Interface Sci.*, 2022, **7**, 21–41.
43 J. Tian, J. Chen, P. Wang, J. Guo, W. Zhu, M. R. Khan, Y. Jin, J. Song and O. J. Rojas, *Green Chem.*, 2023, **25**, 3671–3679.
44 Y. Zhu, S. Huan, L. Bai, A. Ketola, X. Shi, X. Zhang, J. A. Ketoja and O. J. Rojas, *ACS Appl. Mater. Interfaces*, 2020, **12**, 11240.
45 K. Zhang and H. Liimatainen, *Small*, 2018, **14**, 1801937.
46 G. Chu, G. Vasilyev, D. Qu, S. Deng, L. Bai, O. J. Rojas and E. Zussman, *Langmuir*, 2020, **36**, 979–985.
47 E. Kontturi, P. Laaksonen, M. B. Linder, Nonappa, A. H. Gröschel, O. J. Rojas and O. Ikkala, *Adv. Mater.*, 2018, **30**, 1703779.
48 J. Meng, Y. Liu, X. Shi, W. Chen, X. Zhang and H. Yu, *Sci. China Mater.*, 2020, **64**, 621–630.
49 M. Hasani, E. D. Cranston, G. Westman and D. G. Gray, *Soft Matter*, 2008, **4**, 2238–2244.
50 M. Visanko, H. Liimatainen, J. A. Sirviö, J. P. Heiskanen, J. Niinimäki and O. Hormi, *Biomacromolecules*, 2014, **15**, 2769.
51 J. Li, J. F. Revol and R. Marchessault, *J. Appl. Polym. Sci.*, 1997, **65**, 373–380.
52 Z. Zhang, C. Wang, Q. Wang, Y. Zhao and L. Shang, *Proc. Natl. Acad. Sci. U. S. A.*, 2022, **119**, e2204113119.
53 W. Liu, C. Zhang, R. Alessandri, B. T. Diroll, Y. Li, H. Liang, X. Fan, K. Wang, H. Cho, Y. Liu, Y. Dai, Q. Su, N. Li, S. Li, S. Wai, Q. Li, S. Shao, L. Wang, J. Xu, X. Zhang, D. V. Talapin, J. J. Pablo and S. Wang, *Nat. Mater.*, 2023, **22**, 737–745.
54 H. Hu, X. Zhang, W. Liu, Q. Hou and Y. Wang, *Chem. Eng. J.*, 2023, **474**, 145980.
55 S. Matsumura, S. Kajiyama, T. Nishimura and T. Kato, *Small*, 2015, **11**, 5127–5133.
56 C. C. Thong, D. C. L. Teo and C. K. Ng, *Constr. Build. Mater.*, 2016, **107**, 172–180.
57 D. N. Chigrin and C. M. S. Torres, *Opt. Spectrosc.*, 2001, **91**, 484–489.
58 L. Bai, S. Huan, Y. Zhu, G. Chu, D. J. Clements and O. J. Rojas, *Annu. Rev. Food Sci. Technol.*, 2021, **12**, 383–406.
59 L. Bai, S. Huan, O. J. Rojas and D. J. Clements, *J. Agric. Food Chem.*, 2021, **69**, 8944–8963.
60 Y. Huang, H. Liu, S. Liu and S. Li, *J. Agric. Food Chem.*, 2020, **68**, 14620–14631.
61 Y. Zhang, Z. Chen, W. Bian, L. Feng, Z. Wu, P. Wang, X. Zeng and T. Wu, *Food Chem.*, 2015, **183**, 115–121.
62 L. Bai, S. Huan, W. Xiang, L. Liu, Y. Yang, R. W. N. Nugroho, Y. Fan and O. J. Rojas, *ACS Sustainable Chem. Eng.*, 2019, **7**, 6497–6511.
63 S. Huan, Y. Zhu, W. Xu, D. J. Clements, L. Bai and O. J. Rojas, *ACS Appl. Mater. Interfaces*, 2021, **13**, 12581–12593.